SAND2016-4775C

Using a Few Spectral Wavelengths to Enhance Short Circuit Current Predictions in PV Performance Models

Matthew Lave and Clifford Hansen
Sandia National Laboratories, Livermore, CA and Albuquerque, NM

Yuzuru Ueda,
Tokyo Institute of Technology, Tokyo, Japan

Keiichiro Hakuta
NTT Facilities Inc, Tokyo, Japan

***Abstract* — Short circuit current (Isc) depends on the effective irradiance incident upon a PV module. Effective irradiance is highly correlated with broadband irradiance, but can vary slightly as the spectral content of the incident light changes. We explore using a few spectral wavelengths with broadband irradiance to predict Isc for ten modules of varying technologies (silicon, CIGS, CdTe). The goal is to identify a few spectral wavelengths that could be easily (and economically) measured to improve PV performance modeling.**

I. Introduction

Short circuit current (Isc) is important part of I-V curve modeling in PV performance assessment, as it represents the maximum current that could be drawn from the PV cell. Changes in Isc are almost exclusively due to changes in the effective irradiance incident on the module. While effective irradiance is highly correlated with broadband irradiance measured by a pyranometer, subtle differences in spectral content can also impact the effective irradiance since PV modules do not absorb all spectral wavelengths evenly.

In this paper, we explore the relationship between spectral changes and changes in Isc. We look at different module technologies, which have different spectral absorption properties, to note differences between module types. The goal of this work is to identify a few spectral wavelengths which can explain the majority of the variance in Isc that is not explained by the broadband irradiance. This would enable development of a low-cost sensor which measures only a few spectral wavelengths but, combined with broadband irradiance measurements, is a good predictor of Isc.

II. Data

A. Overview

For this study, we used spectral plane of array (POA) irradiance, broadband POA irradiance, Isc, and cell temperature measurements collected in Los Alamos, NM. All measurements were taken at 5-minute resolution. Isc values from 10 different types of PV modules were used, including mono and polycrystalline silicon, CIGS, and CdTe modules. We used data from the month of October 2012 for this analysis.

Simple visual quality control was applied, such as removing times that were clearly inconsistent between Isc and POA irradiance (i.e., Isc is reduced by 50% over the previous timestamp while POA irradiance is nearly unchanged). Additionally, it was found that the spectrometer data changed timestamps for daylight savings time while the Isc and POA irradiance data did not: their times were realigned by shifting the spectrometer data. Additional data beyond October 2012 exists and could be used for this study, pending quality control.

B. Clear Periods Selection

Only clear periods were considered in this work, for two main reasons: (1) previous related modeling (i.e., the Sandia Array Performance Model [1]) only considered clear periods, and (2) temporal or spatial offsets between the spectral, broadband irradiance, and Isc measurements could lead to slight offsets in the arrival times of cloud shadows. Clear periods were selected using a clear-sky detection algorithm, following the process described in [2].

In addition, only times when the solar altitude angle was greater than 20° were considered. This eliminated potentially errant measurements at low solar altitude angles.

C. Irradiance vs. Isc Offset

An inconsistency between the POA irradiance and Isc measurements was discovered, as shown in Figure 1, which compares Isc and POA irradiance measurements from one of the modules (a polysilicon module). Careful inspection of Figure 1a shows that Isc values tend to peak slightly before solar azimuth of 180° (i.e., a few degrees east of south), while POA irradiance values appear to peak at due south azimuth.

Further evidence of this offset is given in the subsequent plots in Figure 1. In Figure 1b, the quantity Isc divided by POA irradiance is shown to have a dependence on solar azimuth, as it is higher in the morning than in the afternoon. Figure 1c shows that POA irradiance has a symmetric dependence on angle of incidence before and after solar noon, suggesting the POA measurement does not have an offset. Figure 1d shows that Isc measurements at the same angle of incidence are higher in the morning than in the afternoon.

This offset between Isc and POA irradiance is not correlated with cell temperature: PV cell temperature was measured and found to increase until mid-afternoon, then

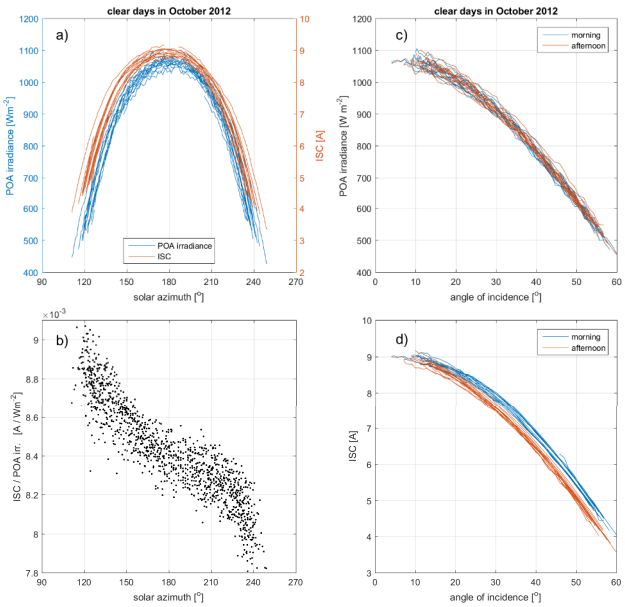

Figure 1: (a) Plot of POA irradiance and Isc as a function of solar azimuth on clear days in October, 2012; (b) Isc divided by POA irradiance; (c) POA irradiance as a function of angle of incidence on a latitude tilt, due south surface; (d) Isc as a function of angle of incidence.

decrease, while Isc is always decreasing relative to POA irradiance. We also do not believe it to be due to a time offset in the measurements since the POA irradiance is measured immediately when the I-V sweep is started and so the Isc and POA measurements should be taken within a few seconds of one another – a roughly 5-minute offset in these measurements would be required to produce the offset seen in Figure 1b.

Thus, a slight azimuth offset is the mostly likely explanation for the behavior seen in Figure 1b. We attempted to find the true azimuth by determining the azimuth angle that led to the smallest variance in the quantity Isc divided by POA irradiance. While this quantity is expected to vary (and in fact that is the point of this project: to use spectral

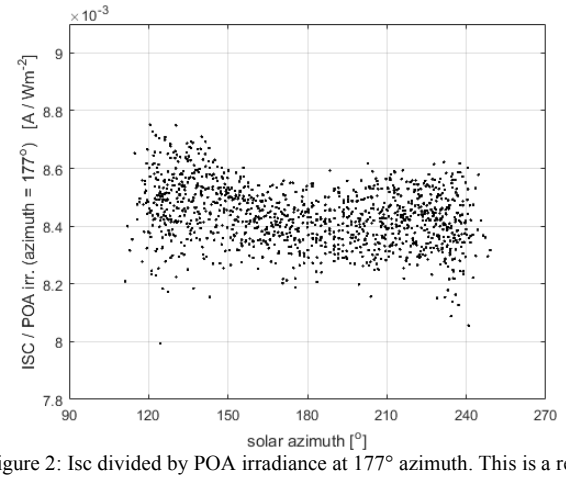

Figure 2: Isc divided by POA irradiance at 177° azimuth. This is a repeat of Figure 1b but with POA irradiance adjusted to the suspected PV module orientation.

predictors to model this variation), we do not expect an azimuth angle dependence. Thus, we feel that the azimuth angle that minimizes the variance is likely the true azimuth. For all 10 modules, the azimuth was found to be 177°±1° (i.e., 2-4° east of south). We feel this could be within the error that could occur during module installation and so is a reasonable explanation of the behavior in Figure 1. Figure 2 shows the Isc divided by POA irradiance relationship for a 177° azimuth, which has much less azimuth angle dependence than Figure 1b.

III. Method

In the Sandia Array Performance Model (SAPM) [1], it is assumed that Isc is a function of air mass, irradiance, and temperature (Equation 1 in [1]). The air mass parameter is meant to be a proxy for changes in the spectral content. Here, we replace the air mass term with measurements from one or more spectral wavelengths. We also remove the temperature dependence to simplify the modeling and due to the typically very small α_{ISC} coefficient [3] indicating that temperature has little impact on I_{sc}. The resulting linear model is of the form:

$$I_{sc} = C_1 + C_2(\text{POA irr}_{az=177°}) + C_3(SP_1 / \text{POA irr}) + \cdots C_{2+n}(SP_n / \text{POA irr}) \quad (1)$$

where $C_1 \ldots C_{2+n}$ are constant multipliers, $\text{POA irr}_{az=177°}$ is the vector timeseries of POA irradiance measurements corrected to true module azimuth of 177°, POA irr is the raw POA measurement at due south azimuth, and each SP_n is a vector containing spectral intensities.

$\text{POA irr}_{az=177°}$ is obtained by multiplying the measured POA irradiance (at due south azimuth) by the ratio of the clear-sky model at 177° azimuth to the clear-sky model at due south azimuth. The SP_n values are the timeseries vector of intensities of irradiance measurements at each wavelength n over the entire study period. For example, SP_{500nm} would be the timeseries of intensities at the 500nm wavelength for all clear days in October 2012. The spectral wavelengths are divided by the POA irradiance so that they can best describe the variation due to spectral changes at similar irradiances (i.e., the variation not explained by irradiance alone).

Important spectral wavelengths were identified using sequential feature selection, which in this case selected a subset of spectral wavelengths that best predicted the Isc values. This was done by minimizing the root mean squared error (RMSE) between the modeled and the actual values of Isc.

For comparison of the impact of other quantities, we additionally evaluated the RMSE for models of the forms:

$$I_{sc} = C_1 + C_2(\text{POA irr}_{az=177°}) + C_3(AM), \quad (2)$$

where AM is air mass,

$$I_{sc} = C_1 + C_2(\text{POA irr}_{az=177°}) + C_3(T_c), \quad (3)$$

where T_c is the measured cell temperature, and

$$I_{sc} = C_1 + C_2(\text{POA irr}_{az=177°}) + C_3(AM) + C_4(T_c). \quad (4)$$

Equation (4) has the same predictors as those used in the SAPM, though in a slightly different model form. This will

allow us to compare the relative value of those predictors to the spectral predictors proposed here.

IV. Results and Discussion

A. One Module: Polycrystalline Silicon

First, we apply Equation (1) with no spectral wavelengths as inputs; that is, we determine a linear model for Isc as a function of only the azimuth = 177° POA irradiance. The resulting model for a polycrystalline silicon module was:

$$I_{sc} = -0.0515 + 0.084 \times \text{POA irr}_{az=177°} \quad (5)$$

and is plotted in Figure 3. The errors shown in Figure 3 are all small: the mean bias error (MBE) of 0.03% shows that the linear model does a good job of describing the overall trend in the data, and the root mean squared error (RMSE) of only 1.24% shows that there is relatively little variation from the linear model. In the rest of this section, we aim to explain this little remaining variation in Isc not described by the POA irradiance. Quantitatively, this means reducing RMSE.

To help understand the relationship between the remaining variance and the spectral intensity at each wavelength, the top plot in Figure 4 shows the spectral intensities divided by the POA irradiance (i.e., SP_1 / POA irr) for each wavelength in the measured spectrum. Each line represents a separate spectral measurement (i.e., a different time), and the color of each line represents the value of Isc/Isc_{model} at that time, where Isc_{model} is the linear irradiance model shown in Equation (5). Thus, vertical color gradients at specific wavelengths indicate correlations between the spectral intensity at that wavelength (relative to the POA irradiance) and the Isc variation from the model in Equation (5). For example, between 400nm and 700nm, the Isc is high relative to the linear irradiance model (yellow colors) when the spectral intensity is high relative to the POA irradiance, and conversely, the Isc is relatively low (blue colors) when the spectral intensity is relatively low. These correlation are plotted explicitly in the bottom plot of Figure 4.

Sequential feature selection was applied to select the most

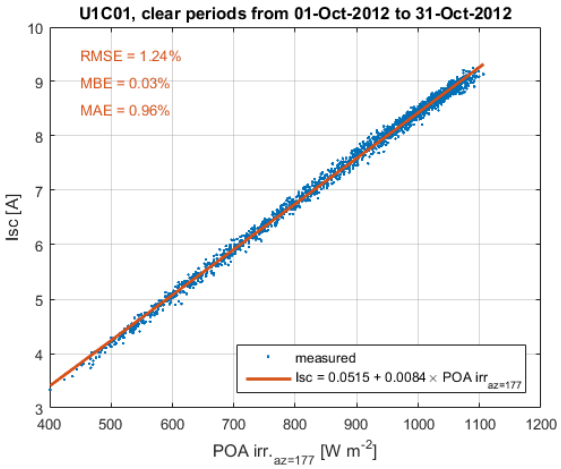

Figure 3: Isc as a linear function of irradiance only for module U1C01, a polycrystalline silicon module. .

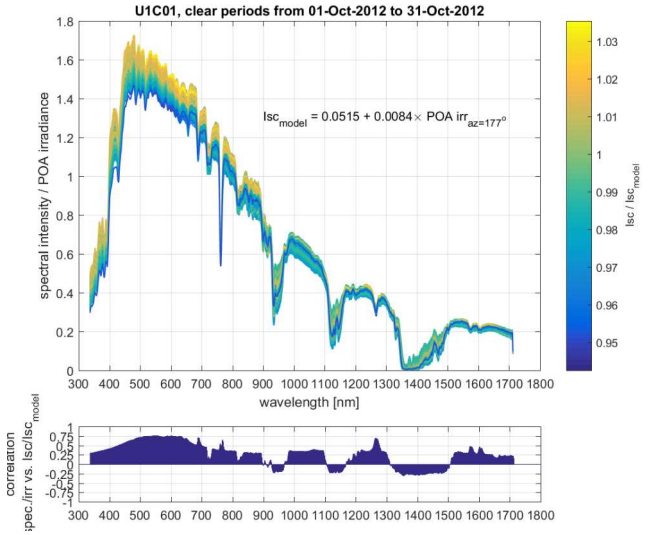

Figure 4: Polycrystalline silicon module. **[Top]** Spectral intensity / POA irradiance, colored by values of Isc / modeled Isc (from Equation (5)). Vertical color gradients (light to dark or dark to light) thus indicate wavelengths at which spectral changes (relative to irradiance) are correlated to Isc changes not described by Equation (5). **[Bottom]** Plot of these correlations – correlation between spectral intensity / POA and Isc / modeled Isc.

important wavelength. The first most important wavelength chosen was 590nm, consistent with the maximum correlation seen in the bottom plot of Figure 4. The new model, with one spectral value, is:

$$I_{sc} = -4.0122 + 0.082 \times \text{POA irr}_{az=177°} + 2.9362 \times (SP_{590nm} / \text{POA irr}). \quad (6)$$

The model in Equation (6) has reduced the RMSE to 0.81%.

We notice that the multiplier on the azimuth = 177° POA irradiance in both the models in Equation (5) and Equation (6) is similar (0.084 and 0.082), showing that the importance importance of broadband irradiance has not waned even when adding the spectral wavelength 590nm. In fact, in their maximum values ($\text{POA irr}_{az=177°} = 1100$, $(SP_{590nm} / \text{POA irr} = 1.7)$, the $\text{POA irr}_{az=177°}$ term is about 18 times larger than the SP_{590nm} / POA irr term ($1100 \times 0.082 = 90.2$ vs. $2.9362 \times 1.7 = 4.99$), which shows the continued strong dependence on POA irradiance that is expected.

It is worth noting that in this sequential feature selection, the second most important wavelength will not necessarily be a wavelength with high correlation in Figure 4. Instead, successive wavelengths chosen will provide orthogonal information to the predictors (POA irradiance and spectral wavelength(s)) already included. The second wavelength predictor chosen was 750nm.

Figure 5 plots the errors and displays error metrics (RMSE, MBE, and MAE) for the Isc models shown in Eqs. (5) and (6) (top two plots). Figure 5 also shows the model errors for models using 2, 3, and 4 spectral wavelengths. Subsequent plots show the errors when using irradiance plus air mass, irradiance plus cell temperature, and irradiance plus air mass and cell temperature (i.e., the same inputs as the SAPM). In shifting from the top left plot in Figure 5 to subsequent plots

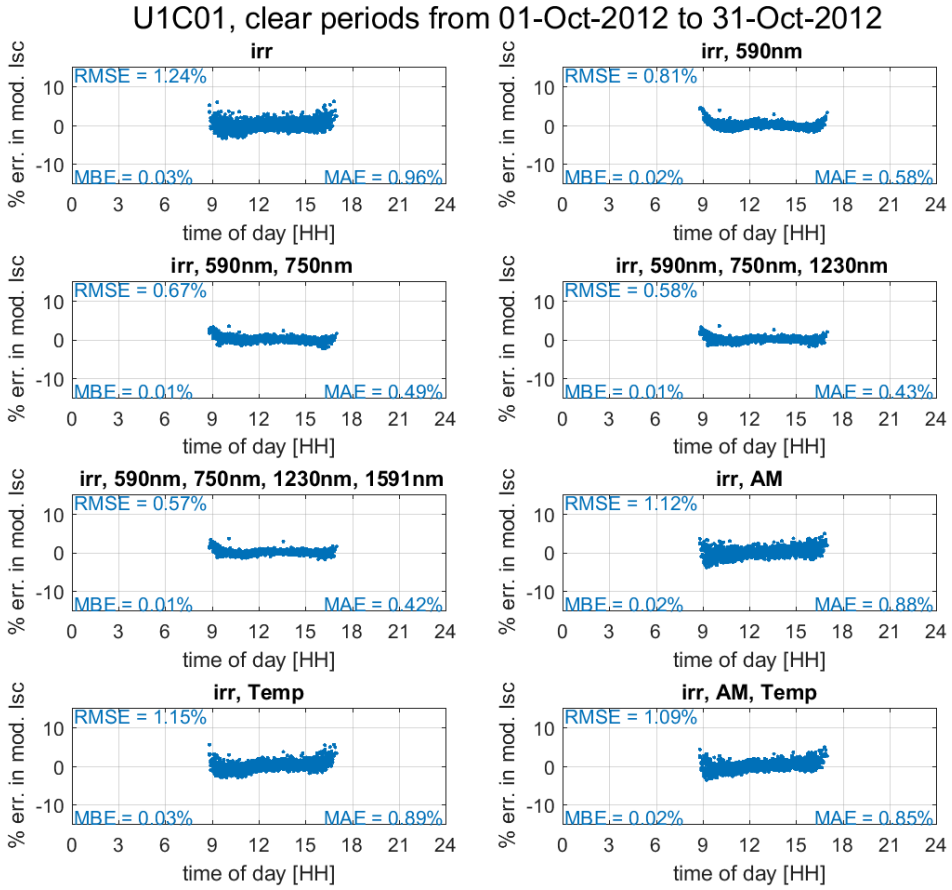

Figure 5: Errors (% of Isc) for irradiance only (top left), irradiance plus spectral wavelengths (top right, middle two, bottom left), and irradiance plus air mass (bottom right).

with spectral predictors, the reduced error shape is evident: adding one spectral predictor reduced the spread of errors; adding two spectral predictors eliminates most of the diurnal variation in the errors. Beyond two predictors, the improvements in error metrics are lesser.

B. All Modules

Figure 6 shows the RMSE errors for all 10 different module types, with zero, one, two, three, or four wavelength predictors. The black lines in Figure 6 show the RMSEs when using the locally optimized spectral wavelengths, optimized individually for each module. Red dashed lines in Figure 6 show the RMSEs when using the globally optimized set of wavelengths that minimized errors across all modules. These globally optimized wavelengths are thus the same for all modules, and show the potential value of measuring a fixed set of wavelengths (rather than specific wavelengths for specific module technologies). Finally, the thin blue dashed lines in Figure 6 show the RMSE when using irradiance, air mass, and cell temperature as predictors.

Just as seen for the single module in Figure 5, all ten modules show value from using additional spectral wavelengths as predictors. However, this value diminishes with each added wavelength: generally the first one or two wavelengths are most valuable; by the fourth added wavelength, very little value is gained.

There is consistency between modules in the most important wavelengths selected. All modules except the bifacial mono Si, single a-Si, and CdTe had a wavelength between 590-592nm as their most important spectral wavelength. Many of the second most important wavelengths are consistent as well. This may suggest that a single sensor measuring only a few wavelengths could be used for spectral corrections to many different types of PV modules.

The red dashed lines in Figure 6 show how sensitive model is to changing the wavelengths used. Most modules have similar RMSE values when using the one wavelength (648nm) from this optimization over all modules as they do from using the first wavelength found in their specific optimization. For all modules, the RMSE when using this 648nm wavelength is smaller than the RMSE from using the traditional air mass and temperature predictors.

To further test the sensitivity of using different wavelengths as predictors, Figure 7 shows the increase in RMSE when using each module's spectral wavelength predictors applied to

other modules for the case when using irradiance plus two spectral wavelengths as predictors.

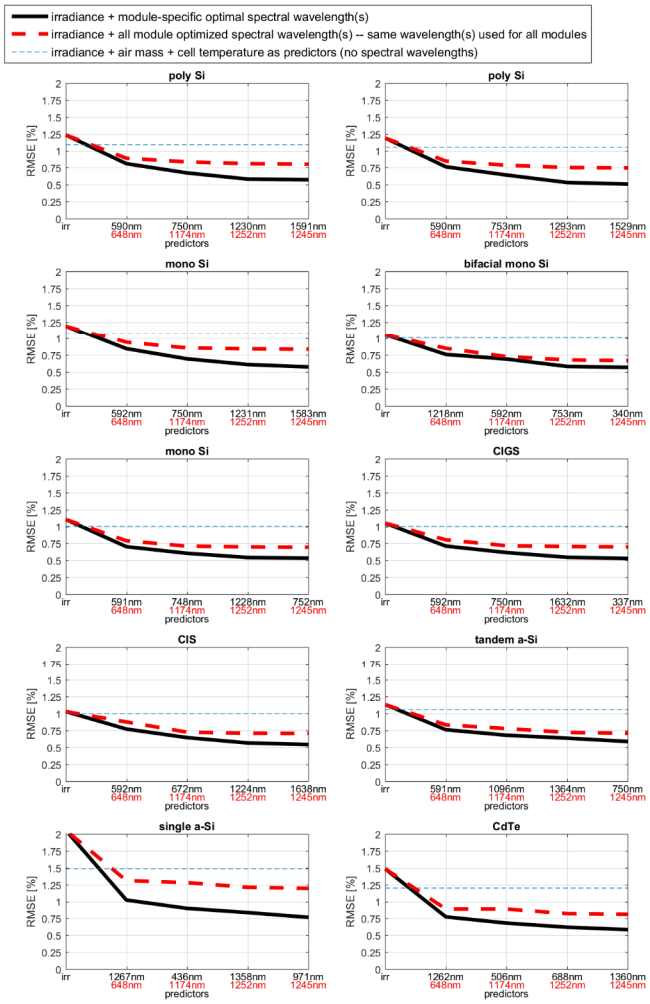

Figure 6: RMSE errors (% of Isc) for each of the 10 different module types. The x-axis shows added predictors (i.e., the second entry includes irradiance plus one spectral wavelength; the last entry includes all four spectral wavelengths as predictors). The black lines show RMSEs when using the optimal wavelengths for each PV technology individually, i.e., wavelengths used change from module to module. The red dashed lines show the RMSEs for the set of wavelengths that minimized errors over all modules, i.e., the wavelengths used are the same for all modules. The thin blue dashed line is the RMSE when using irradiance, air mass, and temperature (but no spectral wavelengths) as predictors.

A few trends are seen in Figure 7. First, when using the wavelengths found for poly Si modules (e.g., 590nm and 750nm as found for the first poly Si module) errors are only slightly increased for all modules except the single a-Si and the CdTe. This is likely caused by the spectral response of these two modules being different than the other modules. Second, related to the first point, errors are increased when using either the single a-Si or CdTe predictors, again likely due to spectral response differences. Finally, errors are large even in the Si modules when using the bifacial mono-Si predictors. The converse (errors in bifacial mon-Si when using other Si predictors), though, does not result in as large

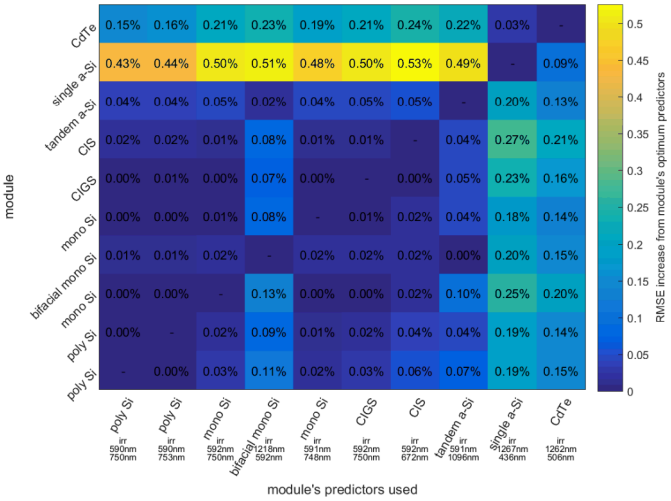

Figure 7: Increase in RMSE when using each different module's predictors instead of a module's optimal predictors, for irradiance plus two spectral wavelengths as predictors. For example, the bottom right grid cell shows that, when using the CdTe predictor wavelengths (1262nm and 506nm), the error in the poly Si module Isc prediction was increased by 0.15% (from 0.67% to 0.82%) compared to the optimal poly Si wavelengths (590nm and 750nm).

of errors. A possible explanation for this is that the bifacial module is sensitive to both wavelengths important to traditional Si modules and also sensitive to a separate wavelength related to the reflected irradiance reaching the side of the module not facing the sun. The former sensitivity would mean that the traditional Si predictors are also good predictors of the bifacial module's Isc, while the later sensitivity would have determined the optimal predictor wavelengths and thus have included a wavelength important to irradiance reaching the back side of the module.

V. Potential Applicability At a Different Location

The methods in this analysis were repeated using data collected at Sandia National Laboratories in Albuquerque, NM. This Albuquerque dataset had several limitations over the Los Alamos data: PV modules were typically only tested for a few days at a time (so long-term analysis is not possible), and broadband irradiance, spectral, and Isc measurements were all collected at different times with different spacing between measurements. An additional difference between the Albuquerque and Los Alamos datasets is that all Albuquerque measurements are collected on a two-axis tracker that is always normal to the sun, rather than the fixed orientation of the Los Alamos measurements.

Despite these differences between the two datasets, we performed a simple to see test whether the important wavelengths found in section IV. For this test we chose the clear day May 27, 2014 in Albuquerque. A longer test period such as the month used for Los Alamos was not possible due to the short Isc collection periods for each module in Albuquerque. Figure 8 shows the spectral correlations for a monocrystalline silicon module in Albuquerque, just as Figure 4 did for the polycrystalline module in Los Alamos.

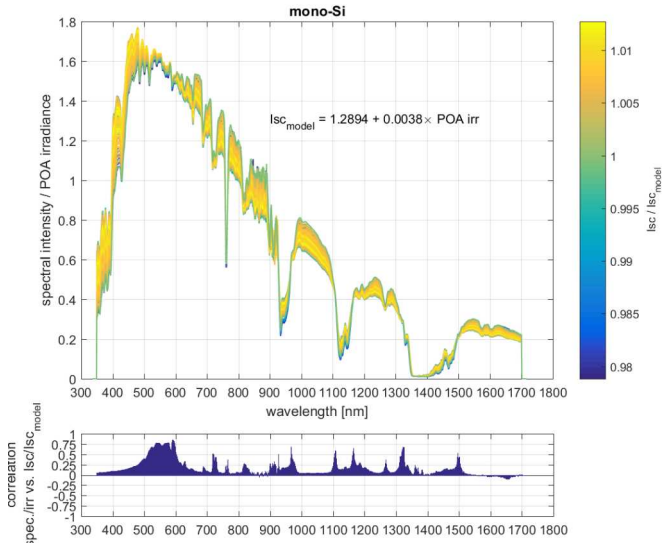

Figure 8: Monocrystalline silicon module in Albuquerque. **[Top]** Spectral intensity / POA irradiance, colored by values of Isc / modeled Isc (from Equation (5)). Vertical color gradients (light to dark or dark to light) thus indicate wavelengths at which spectral changes (relative to irradiance) are correlated to Isc changes not described by Equation (5). **[Bottom]** Plot of these correlations – correlation between spectral intensity / POA and Isc / modeled Isc.

Differences between Figure 4 and Figure 8 may be due to differences is spectral changes between Los Alamos and Albuquerque, though they could also be due to data collection differences (collection times of measurements, fixed tilt vs. two-axis tracking, etc.).

Figure 9 shows the RMSE errors when adding additional spectral wavelength predictors for a monocrystalline silicon module in Albuquerque, analogous to Figure 6. The RMSE errors for the optimum predictors (black line) are smaller than those found in Los Alamos, perhaps because of the coplanar irradiance and Isc measurements in Albuquerque (both are taken on the two-axis tracker), rather than the suspected 3˚ offset between irradiance and Isc measurements in Los Alamos.

Also included in Figure 9 are the wavelengths found to minimize the errors for all Los Alamos modules (red dashed line) and for a monocrystalline silicon module in Los Alamos (blue dashed line). Both are still improvements over irradiance as the only predictor. And, the Los Alamos monocrystalline wavelengths do seem to be better predictors than the general Los Alamos wavelengths, suggesting that may be a geographically independent set of optimal wavelengths for monocrystalline silicon modules. However, due to the limited data analyzed and the inconsistent measurement times in Albuquerque, these results still need further verification.

VI. Conclusions and Further Work

Initial results are promising that a few spectral wavelengths can be added as meaningful predictors of Isc. The analysis has been extended to another location (Albuquerque, NM), and

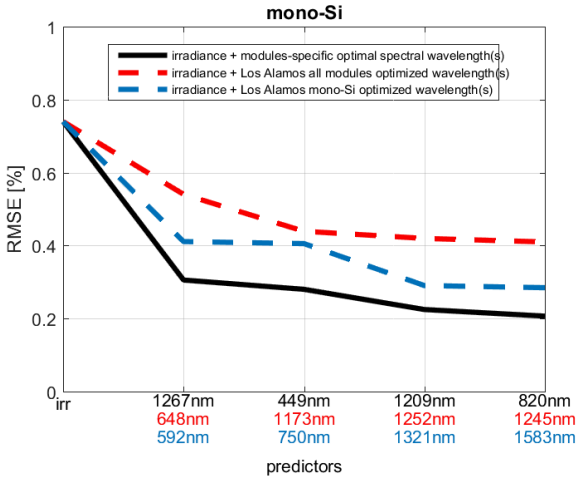

Figure 9: RMSE errors (% of Isc) for a monocrystalline silicon module in Albuquerque. The x-axis shows added predictors (i.e., the second entry includes irradiance plus one spectral wavelength; the last entry includes all four spectral wavelengths as predictors). The black line shows RMSEs when using the optimal wavelengths. The red dashed lines show the RMSEs for the set of wavelengths that minimized errors over all Los Alamos modules. The blue dashed line is the RMSE when using the set of wavelengths found for a monocrystalline silicon module in Los Alamos.

results were found to be consistent in general terms: one or more spectral wavelengths were beneficial as predictors of Isc. Further work could be done to compare other locations, and to test the sensitivity and consistency across different locations or seasons of the spectral wavelengths used as predictors.

Acknowledgment

Data for this work was collected and graciously shared by the New Energy and Industrial Technology Development Organization (NEDO).

Sandia National Laboratories is a multi-program laboratory managed and operated by Sandia Corporation, a wholly owned subsidiary of Lockheed Martin Corporation, for the U.S. Department of Energy's National Nuclear Security Administration under contract DE-AC04-94AL85000. SAND2016-XXXX.

References

[1] D. L. King, J. A. Kratochvil, and W. E. Boyson, "Photovoltaic array performance model," Sandia National Laboratories SAND2004-3535, 2004.

[2] M. J. Reno, C. W. Hansen, and J. S. Stein, "Global Horizontal Irradiance Clear Sky Models: Implementation and Analysis," Sandia National Laboratories SAND2012-2389, 2012.

[3] D. L. King, J. A. Kratochvil, and W. E. Boyson, "Temperature coefficients for PV modules and arrays: measurement methods, difficulties, and results," in *Photovoltaic Specialists Conference, 1997., Conference Record of the Twenty-Sixth IEEE*, 1997, pp. 1183-1186.